HHS Public Access

Author manuscript

Anal Chem. Author manuscript; available in PMC 2018 January 03.

Published in final edited form as:

Anal Chem. 2017 January 03; 89(1): 862–870. doi:10.1021/acs.analchem.6b03926.

Spectral and Hydrodynamic Analysis of West Nile Virus RNA—Protein Interactions by Multiwavelength Sedimentation Velocity in the Analytical Ultracentrifuge

Jin Zhang[†,‡,▽], **Joseph Z. Pearson**[§], **Gary E. Gorbet**[‖], **Helmut Cölfen**[§], **Markus W. Germann**[†,‡], **Margo A. Brinton**[‡], and **Borries Demeler**[*,‖]

[†]Georgia State University, Department of Chemistry, 50 Decatur St. SE, Atlanta, Georgia 30303, United States

[‡]Georgia State University, Department of Biology, P.O. 4010, Atlanta, Georgia 30303, United States

[§]University of Konstanz, Department of Chemistry, Physical Chemistry, Universitätsstraße 10, Box 714, D-78457 Konstanz, Germany

[‖] The University of Texas Health Science Center at San Antonio, 7703 Floyd Curl Drive, MC 7760, San Antonio, Texas 78229-3901, United States

Abstract

Interactions between nucleic acids and proteins are critical for many cellular processes, and their study is of utmost importance to many areas of biochemistry, cellular biology, and virology. Here, we introduce a new analytical method based on sedimentation velocity (SV) analytical ultracentrifugation, in combination with a novel multiwavelength detector to characterize such interactions. We identified the stoichiometry and molar mass of a complex formed during the interaction of a West Nile virus RNA stem loop structure with the human T cell-restricted intracellular antigen-1 related protein. SV has long been proven as a powerful technique for studying dynamic assembly processes under physiological conditions in solution. Here, we demonstrate, for the first time, how the new multiwavelength technology can be exploited to study protein—RNA interactions, and show how the spectral information derived from the new detector complements the traditional hydrodynamic information from analytical ultracentrifugation. Our method allows the protein and nucleic acid signals to be separated by spectral decomposition such that sedimentation information from each individual species, including any complexes, can be

[*]**Corresponding Author:** Tel.: 210-767-3332. Fax: 201-567-6595. demeler@biochem.uthscsa.edu.

[▽]**Present Address:** Beijing University of Technology, Beijing Advanced Innovation Center for Soft Matter Science and Engineering, North Third Ring Road 15, Chaoyang District, Beijing, 100029, PRC.

ORCID

Borries Demeler: 0000-0002-2414-9518

Supporting Information

The Supporting Information is available free of charge on the ACS Publications website at DOI: 10.1021/acs.anal-chem.t6b03926.

Method details and additional figures (PDF)

Movies of the four-dimensional MWL-AUC data (ZIP)

Notes

The authors declare no competing financial interest.

clearly identified based on their spectral signatures. The method presented here extends to any interacting system where the interaction partners are spectrally separable.

Graphical Abstract

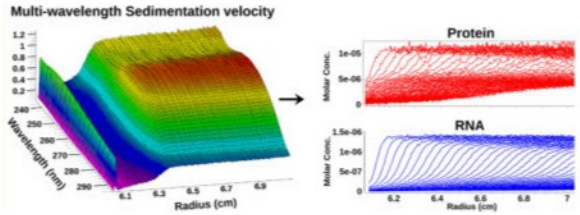

Interactions between proteins and nucleic acids are at the core of many cellular processes. For example, more than 10% of cell proteins are RNA binding proteins,[1] and nuclear DNA interacts with histones, regulatory proteins, and the replication machinery. Numerous methods have been devised to study these interactions. X-ray crystallography and nuclear magnetic resonance (NMR) spectroscopy may provide atomistic models of an entire complex,[2–5] and help identify binding interfaces, but these methods are time and resource intensive and require well-behaved systems. Consequently, relatively few structures of protein—RNA complexes have been solved to date. Other methods, such as surface plasmon resonance, isothermal titration calorimetry, and fluorescence anisotropy, can be used to study the thermodynamics of interactions. However, each method brings its own limitations, be it resolution, size restrictions on the analyte, sample requirements, or absence of physiological conditions during the measurement. Here, we introduce a new approach for studying protein—nucleic acid interactions, which promises to provide new details in the characterization of assembly processes, helps to identify the stoichiometry of the interaction, and characterize the thermodynamic properties of reversible complexes. The approach employs analytical ultracentrifugation (AUC) and sedimentation velocity (SV), and uses a novel multiwavelength analytical ultracentrifugation (MWL-AUC) detector,[6,7] in combination with high-performance computing (HPC), to evaluate the data. AUC has long been regarded as the gold standard for studying macromolecular assemblies and complexes in solution, because the physiological conditions found in the cytosol can be approximated during the experiment. Factors, such as ionic strength, pH, reduction potential, presence of nucleotides, small molecules and drugs, can easily be manipulated. During AUC experiments, solutes are separated in a centrifugal force field based on their hydrodynamic properties, which provides access to each solute's partial concentration, anisotropy, and mass. The experimental data represent the evolution of each solute's concentration gradient over radius and time. These data are typically fitted to finite element solutions of the Lamm equation,[8–10] which describe the sedimentation and diffusional flow in the ultracentrifuge cell. A series of optimization approaches, developed in the Demeler laboratory, are used together with HPC programs to find models that describe the experimental data.[11–19]

In traditional AUC instruments, data are collected by either observing the ultraviolet (UV) or visible (Vis) absorbance at a single wavelength, or by measuring Rayleigh interference, or fluorescence emission intensity. The UV absorbance optics in the Beckman Optima XL-I allows collection of up to three wavelengths, with simultaneous Rayleigh interference data

collection, but the reproducibility of wavelength measurements is so unreliable that, for all practical purposes, it is hardly useful. Nevertheless, a considerable body of work exists for studying nucleic acid—protein interactions in solution using analytical ultracentrifugation with multiple signals (for representative examples, the reader is referred to refs [20–22]). Because of the lack of precision in the wavelength reproducibility in the Beckman instrument, most applications focusing on multisignal analysis employ sedimentation equilibrium experiments, which can more easily be corrected for wavelength variation.[23] Previously, multisignal analysis of SV experiments combined Rayleigh interference data with UV absorbance to study protein—RNA interactions,[24] or focused on protein mixtures;[25] however, because of hardware limitations, spectral resolution is rather low. In the case of protein—nucleic acid interactions, little is gained when interference signal is added. First, the concentrations required for interference experiments are rather high and are not necessarily compatible with the dynamic range of the UV detector at the peak wavelengths; second, the refractive indices of proteins and nucleic acids are impossible to deconvolute from a single measurement at a single wavelength. However, single-wavelength studies have been successfully used to study protein—RNA associations by analyzing different titrations in the analytical ultracentrifuge, using SV alone[26] or combined with sedimentation equilibrium methods;[27] however, the signals from protein and nucleic acids cannot be separated. In this work, we combined protein—RNA titrations with our multiwavelength analysis approach, where an entire wavelength range of interest can be monitored. Previously, we have demonstrated the significant improvement in resolution obtained with this approach when it is applied to heterogeneous, noninteracting protein and nucleic acid mixtures (see Figure 7 in ref 28, which contrasts the results obtained by using 2 wavelengths in the XL-A versus 60 wavelengths in the MWL-AUC). By introducing a second dimension of observation—the spectral absorptivity of all components in a mixture —it is now possible to detect different solutes that are not only based on their hydrodynamic differences, but also are based on their UV-Vis absorbance spectra. MWL-AUC data can be decomposed into separate datasets based on the spectral signals of individual components, which can then be analyzed individually.[28] If different chemical substances present in a mixture possess unique chromophores, giving rise to separable spectral signals, then the identity and molar amount of these substances can be resolved based on their known molar extinction profiles. In such a case, the absorbance spectrum from each substance adds important new and complementary information to the traditionally obtained hydrodynamic information on an AUC experiment. As was demonstrated previously,[28] the spectral profiles of proteins and nucleic acids are sufficiently different to allow quantifying mixtures by deconvolution of the overlapping spectra. In the previous study, a spectral range of 240–300 nm was sufficient to completely resolve a plasmid DNA digest mixed with bovine serum albumin, even though the sedimentation signal of the two analytes overlapped significantly.

Given the advances in methodology, we investigated the interaction of human T cell-restricted intracellular antigen-1-related protein (hTIAR) and a West Nile virus (WNV) RNA 3′ stem loop structure, (WNV-RNA) (Figure 1). WNV is a flavivirus and a human pathogen that causes significant human morbidity and mortality in ever-expanding regions of the world. Currently, no effective antiviral atherapies exist. hTIAR possesses three RNA recognition motifs (RRMs) and a C-terminal prion domain.[29–32] hTIAR and the closely

related protein TIA-1 are involved in regulating alternative pre-mRNA splicing, nucleating stress granule assembly, and regulating cell translation. In the latter role, hTIAR binds to AU-rich sequences in long single-stranded regions of the 3′ untranslated regions (UTRs) of some mRNAs and to CU-rich regions in the 5′ UTRs of others.[33–35] Although the structures of individual RRM domains of hTIAR have been reported, no highresolution structure of hTIAR in complex with an oligonucleotide has been reported and the precise structural basis for single-stranded RNA binding is not known. Our previous work has shown that hTIAR binds to the central loop region of the 3′ terminal stem loop structure of the negative strand of WNV 3′(−) SL[36] (Figure 1). This interaction is novel, involves multiple assembly steps, and facilitates the synthesis of the WNV genome (the positive strand) RNA.[37,38] This essential cellular protein-viral RNA interaction therefore adds a target for future design of broad spectrum antiflavivirus therapies. Here, we investigate the nature of the cell protein—viral RNA interactions using MWL-AUC to gain insights into the molecular mechanisms by which the recruiting of hTIAR regulates WNV plus strand RNA synthesis. In this study, hTIAR with a molar mass of 31.9 kDa and a 75-nucleotide RNA structure from the 3′ terminal of the WNV minus strand RNA, WNV 3′(−) SL (WNV-RNA), with a molar mass of 23.8 kDa, were selected as interaction partners.

MATERIALS AND METHODS

Protein and RNA Preparation

hTIAR was expressed as a recombinant protein fused to an N-terminal Glutathione-S-transferase tag (GST) in *Escherichia coli* strain Rosetta 2(DE3) pLysS cells (Novagen). Cells were incubated until an optical density of 0.6–0.7 at 600 nm was reached. After overnight post-induction at 20 °C, cells were harvested by centrifugation. Cell pellets were lysed with protease inhibitor cocktail tablets (Roche). The lysate was centrifuged at 12 000*g* for 30 min at 4 °C. Proteins remaining in the lysate supernatant were salted out with ammonium sulfate to a final concentration of 70% (w/v) and pelleted with centrifugation, and resuspended in PBS buffer. The GST tag was removed by addition of the site-specific protease PreScission Protease (GE Healthcare) and further purified by gel filtration. WNV-RNA was produced by transcription from a PCR amplified dsDNA template. The RNA transcript was isolated by anion exchange column and desalted. Further details are available in the Supporting Information.

Isothermal Titration Calorimetry

Reaction heats of dialyzed hTIAR and WNV-RNA samples were recorded using a VP-ITC Microcalorimeter (GE Healthcare, Inc.) with a stirring rate of 310 rpm and a reference power of 18 μcal/s at 25 °C. The isotherms were corrected for the heats ofprotein or RNA dilution by subtracting the average of 3–5 data points from the saturated tail of the titration. The titration was made by injections of 8 μL of protein solution (78 μM) over a period of 16 s into the RNA solution (initial concentration = 3.5 μM) with a 5 min interval between subsequent injections. Further details are available in the Supporting Information.

Multiwavelength Analytical Ultracentifugation (MWL-AUC)

Purified hTIAR and WNV-RNA were measured separately as controls and were mixed in molar ratios of 3:1, 6:1, and 10:1 with a constant concentration of 1.2 μM RNA and sedimented in a MWL-AUC equipped analytical ultra-centrifuge at the University of Konstanz (Germany), as described in refs [6, 7], and [39]. This detector is installed into a preparative Beckman Model XL-80K ultracentrifuge equipped with a XL-I heatsink. The detector itself is based on a Model USB 2000 CCD array spectrometer (Ocean Optics), which allows the acquisition of full UV-vis spectra in the range of 230–700 nm on a 2048 pixel array within 1 ms for a single spectrum. The white light from a xenon flash lamp is guided into the rotor chamber via optical fibers and a vacuum feedthrough. The entire detector is mounted on a detector arm. The complete multiwavelength hardware design is shown in Figure SI4 in the Supporting Information (available for free download as part of the Open AUC project at: http://wiki.bcf2. uthscsa.edu/openAUC). The buffer contained 10 mM sodium phosphate, 50 mM NaCl, and 1 mM TCEP. Samples were spun at 20 °C in standard 12 mm titanium two-channel centerpieces (Nanolytics, Potsdam, Germany) at 60 000 rpm. Spectra in the range from 236 nm to 294 nm were recorded in 1 nm increments (59 individual datasets for each titration point). All data were analyzed with UltraScan-III, release 2021,[40,41] and all figures were prepared with UltraScan. Movies of the four-dimensional MWL-AUC data (intensity converted to pseudo-absorbance, as a function of time, radius, and wavelength) are provided in the Supporting Information.

Data Analysis

All MWL-AUC data were analyzed by the two-dimensional spectrum analysis (2DSA),[11,12] which provides an unbiased hydrodynamic model for the datasets obtained at each wavelength. The 2DSA allows floating the anisotropy (f/f_0) and sedimentation coefficient independently, and it provides for the removal of time-invariant and radially invariant noise components, as well as fitting of the meniscus position. For selected datasets, genetic algorithm analysis was used to further refine the 2DSA result. In this approach, solutes found in the 2DSA are parsimoniously regularized to satisfy Occam's razor, and to optimize their positions in the two-dimensional parameter space of anisotropy and size as described in ref 13. The partial specific volume for hTIAR was predicted based on the amino acid composition using UltraScan; buffer density and viscosity were predicted based on the buffer composition using UltraScan. Absorbance spectra for pure hTIAR, WNV-RNA, and buffer were obtained by measuring a dilution series of each pure component using a Genesys 10s benchtop spectrophotometer (Thermo Scientific). Spectral profiles generated with the benchtop spectrophotometer were compared to those observed in the MWL-AUC and found to be identical in shape and peak position, although having less noise (see Figure SI5 in the Supporting Information). The dilution series were fitted to intrinsic extinction profiles as described in ref 28. The resulting profiles were scaled to molar concentration using an extinction coefficient of 33 720 M^{-1} cm^{-1} at 280 nm for hTIAR, as predicted by UltraScan from the amino acid sequence. For WNV-RNA, an extinction coefficient of 732 400 M^{-1} cm^{-1} at 260 nm was determined by the nearest-neighbor method.[42,43] The scaled profiles were then used to decompose the noise-corrected MWL-AUC data into three separate three-dimensional (3D) datasets (molar concentration as a function of radius and time), using the non-negatively constrained least-squares (NNLS) algorithm;[44] further details on this

procedure can be found in ref 28. Briefly, for each radius position and for each time point, the MWL-AUC instrument provides an entire wavelength scan that can be decomposed into a sum of absorbance spectra, resulting in an amplitude scalar for each component. This can be written in matrix form as

$$\mathbf{Ax}=\mathbf{b}_{r,t}$$

where **A** is the matrix containing the spectral contributions from each component, **x** the vector of amplitudes for each component, and **b** the wavelength scan at radius point *r* and scan *t*. By fitting this equation for each *r* and *t*, one new synthetic, 3D MWL-AUC dataset was created for each component contained in **A**, where the number of new datasets corresponds to the number of columns in **A.** By using the NNLS algorithm for this fit, the result is constrained to values greater than zero, avoiding the risk of negative contributions possible in the decomposition algorithm used by Walter et al.[45] This process is illustrated in Figure 2. Here, it is important that the columns of **A** are linearly independent; in other words, the absorbance spectrum for each component must be sufficiently different to guarantee linear separation. A convenient metric for the linear dependence is the vector angle α between two spectra u and v, given by

$$\alpha=\cos^{-1}\left[\frac{u\cdot v}{||u||\cdot||v||}\right]$$

where an angle of 0° reflects linear dependence, or perfect overlap of two basis spectra, and an angle of 90° indicates perfect orthogonality, or no spectral overlap at all.[45] For the spectra of hTIAR and WNV RNA, α was found to be 46.4°, whereas for buffer and hTIAR, α was found to be 34.4°, and for buffer and WNV-RNA, α was found to be 72.2°. In theory, any angle larger than 0° offers linear independence between the spectra, and guarantees spectral separability, but the greater the angle, and the greater the wavelength range, the more reliably different spectra can be separated. For nucleic acid and protein spectra, separability is helped by the inclusion of a large number of wavelengths, where the spectral profiles differ, despite some overlap of the chromophores. Individual datasets resulting from the NNLS decomposition were analyzed by conventional means available through UltraScan, as described in ref 46. Next, the hTIAR and RNA datasets obtained above for different mixing ratios were fitted globally to a 2DSA-Monte Carlo solution.[16] The highest hTIAR:RNA titration ratio (10:1) was also fitted to a global genetic algorithm solution. By globally fitting both the protein and RNA datasets simultaneously, a solution is found that fits all hydrodynamically distinct components present in both hTIAR and WNV-RNA datasets to a common distribution of sedimentation and diffusion coefficients, corresponding to the size and anisotropy of any solutes present in either sample. The global model will then contain the same solute species in models describing both datasets, but the amplitudes for each solute in the model may be different for each dataset. When a solute is not found in one of the datasets, its amplitude is set to zero. A solute found in more than one dataset indicates that this solute represents a complex with all other species that share the same hydrodynamic parameters. Since extinction coefficients can be quite different for RNA and protein,

amplitudes must allow for variable ratios between different hydrodynamic species in each dataset.[41] The TCEP dataset was not further analyzed because it only contributes to a nonsedimenting baseline offset; however, by including the TCEP absorbance in the wavelength decomposition, the UV contributions from TCEP were taken into account and did not distort the UV signals attributed to hTIAR and WNV-RNA. Since the multiwavelength detector records intensity measurements, buffer absorbance is not subtracted and must be considered in the wavelength decomposition process. Once the absorption signal is converted to molar concentration, the amplitudes of species involved in complexes allow calculation of molar ratios between species and directly provide the molar stoichiometry of the complex. Sedimentation coefficient distributions obtained from globally fitted 2DSA-Monte Carlo analyses, scaled for molar concentration, are shown in Figure 3.

RESULTS

Separated signals for protein and nucleic acid were obtained from MWL-AUC experiments of hTIAR-WNV-RNA mixtures at different molar ratios. Figure 3 shows the sedimentation coefficient distributions for 2DSA-Monte Carlo analyses from pure hTIAR and WNV-RNA controls, as well as protein—RNA mixtures with loading ratios of 3:1, 6:1, and 10:1. The protein control was measured at the highest concentration used in the titration experiment (11.6 μM) and showed no signs of self-association when sedimented by itself. This observation is further supported by size exclusion chromatography experiments which show a single monomeric species (see Figure SI6 in the Supporting Information). When hTIAR and WNV-RNA are mixed, results clearly show a co-migration of the protein and RNA signals, which demonstrates complex formation. Integration of the co-migrating peaks provides direct access to the stoichiometry and hydrodynamic properties of the solutes that correspond to the complex formed. Detailed results are listed in Table 1.

We found that the size of the complex changes as a function of protein concentration, suggesting subsaturation at the 3:1 and 6:1 molar mixing ratios. At the 10:1 mixing ratio, the complex no longer increases in size, but the distribution is considerably more narrow, suggesting that a stable complex is formed. Integration of the peaks in the co-migrating regions for each loading ratio suggested a series of assembly steps starting with a mostly 2:1 molar ratio hTIAR:WNV-RNA complex at a 3:1 loading, forming a broad reaction boundary reflecting multiple species, with a peak centered at ~6.43 S. Upon increasing protein concentration to a 6:1 loading ratio of protein:RNA, this peak shape remains broad, but shifts to a higher sedimentation coefficient of 7.69 S. Integration of this peak suggests a 4:1 hTIAR:WNV-RNA complex. Increasing the protein concentration further to a 10:1 loading ratio, the 4:1 hTIAR:WNV-RNA ratio does not change, although the sedimentation coefficient increases and the peak becomes narrow and well-defined at 8.78 S. Also, in the protein dataset, a new peak appears that is congruent with the free protein control, suggesting the presence of excess unbound protein. The increased broadness and slightly lower sedimentation coefficient of the 7.69 S species in the 6:1 loading ratio system is indicative of the reaction boundary of complex formation still at subsaturation, where multiple intermediates may be present due to mass action effects, while the narrow 8.78 S peak suggests a stable end point of the titration complex. This is further supported by the appearance of the free protein species, which indicates that excess protein is present, and no

free RNA remains to be complexed. The emergence of a pattern that points to discrete species (a stable complex and free protein) suggests that the 10:1 titration is suitable for global genetic algorithm analysis. The results of the genetic algorithm analysis for the 10:1 titration are shown in Figure 4, and numerical results are shown in Table 1. Because the shapes of the *s*-value distributions from protein and RNA closely track across the reaction boundary, estimated stoichiometries in the reaction boundary strongly suggest complex formation. This effect gives rise to multiple, dynamic oligomerization states, which can result in noninteger peak integration ratios (Table 1). Since multiple species are possible in the broad reaction boundary, the integration ratios represent averages of all species in the boundary. Hydrodynamic integration is consistent with a tetramer of hTIAR bound to one WNV-RNA molecule, and is in excellent agreement with the 4:1 molar ratio of the 8.78 S species. A partial specific volume consistent with this 4:1 ratio permits calculation of the absolute molar mass of the complex from the hydrodynamic data (Table 1), revealing a molar mass of 152.7 kDa. In addition, in the 10:1 titration, we observed a second protein peak that does not exhibit any co-migrating RNA signal. Furthermore, this peak is at the same position as free hTIAR, suggesting that this peak is, in fact, free protein, and the hTIAR:WNV-RNA complex is saturated at this point and remains a stable 4:1 protein:RNA species. We could not find evidence of significant amounts of free RNA, indicating tight binding. To further validate the binding event, we performed isothermal titration calorimetry (ITC). Here, the sequential assembly of the complex was also evident in the ITC isotherm of hTIAR:WNV-RNA, where the heat of the binding reaction was monitored when hTIAR was titrated into the sample cell containing WNV-RNA (Figure SI7 in the Supporting Information). The shape of the reaction enthalpy curve indicates a complex, multistage binding reaction, never reaching a plateau (up to 5.5:1 molar ratio tested). This is fully consistent with the MWL-AUC data, which show a broad reaction boundary with a gradual shift of the sedimentation coefficient to a stable 8.78 S species only when protein concentration is increased to a 10:1 protein:RNA ratio.

DISCUSSION

We demonstrated that MWL-AUC offers a powerful new tool for the analysis of interacting systems, where the individual components have distinct chromophores. We showed that the additional spectral dimension measured here offered critical information about the molar ratios of the complex-forming constituents that is complementary to the hydrodynamic information obtained from the separation of the species by AUC, and aids greatly in the characterization of the species identified by SV analysis. We show that the separation of the protein and nucleic acid signal allowed us not only to determine the ratio of RNA to protein in various species sedimenting with different sedimentation coefficients, but also simultaneously demonstrate that, when the spectrally determined molar ratio is unchanged, that the hydrodynamic data clearly can differentiate between a 4:1 and 8:2 species. In cases where multiple assembly products are possible, MWL-AUC data are now able to provide more-detailed insights into the assembly process and allow the investigator to distinguish between multiple possibilities that would otherwise be consistent with the same hydrodynamic data. We note a limited ability to interpret the broad reaction boundaries observed under subsaturating conditions. A true reaction boundary implies the presence of

free RNA. Yet, we cannot observe the presence of free RNA, suggesting that the concentration of free RNA is very low, or nonexistent. This leaves the true composition of reaction boundaries open for interpretation. Clearly, a reaction is occurring, because significant shifts in S are observed, and a co-migration of protein and RNA are clear from the spectral results. For that reason, we suspect that the K_d for binding between RNA and protein is quite low and is beyond the detection capability of the new instrument, which would suggest that the broad boundaries observed under nonsaturating conditions are caused by the presence of different species with varying ratios of RNA and protein, and all free RNA is always sequestered by the protein present in solution.

For the interaction partner hTIAR and WNV-RNA, MWL-AUC analysis revealed the dependence of the complex formation on the relative concentration of the protein and RNA molecules. In addition, the multistep assembly process elucidated from MWL-AUC analysis suggested that the lower-order complex may be necessary and critical for the formation of the higher-order complex. Given that recent preliminary data showed that stable overexpression of hTIAR enhanced the ratio of WNV positive strand to negative strand levels, our result suggests that the virus may take advantage of the ability of this cellular protein to form a stable complex with the WNV-RNA. The new results on the binding of hTIAR to the WNV-RNA provide mechanistic insights that can be further tested.

Note that the possibility for chromatic shifts upon complex formation exists, especially in the case of nucleic acids that may exhibit base stacking rearrangements upon binding and may present heterogeneity in conformation, leading to uncertainty in the extinction coefficient. Any changes in the spectral profile upon binding would cause systematic errors during deconvolution detectable in the residuals. However, such effects were not observed in the study presented here; hence, we expect negligible conformational changes of the RNA upon interaction with protein. This expectation is further supported through structural observations with NMR. Nevertheless, the reader should be cautioned that any errors in the estimation of the extinction coefficients will distort the molar ratios of any species observed, and may lead to incorrect conclusions about the stoichiometry of associations. In addition to protein—nucleic acid systems, we propose that this technique can be applied to a great variety of systems, where distinct absorption properties can be exploited. Molecules amenable for the analysis described herein may contain hemes, flavins, fluorescent tags, fluorescent protein fusions, proteins with different ratios between peptide bond, and aromatic amino acid side chain absorbance, and other unique chromophores, such as those that may be found in small molecules and drugs. This will be of great value when drug—protein or drug—nucleic acid interactions are investigated.

Supplementary Material

Refer to Web version on PubMed Central for supplementary material.

Acknowledgments

This study was supported by Public Health Service Research Grant No. AI048088 to M.A.B. from the National Institute of Allergy and Infectious Diseases, National Institutes of Health and NIH (Grant No. GM-120600) to B.D., and by the National Science Foundation (Grant No. ACI-1339649) to B.D.; computer time on XSEDE resources

was funded by National Science Foundation allocation Grant No. TG-MCB070039N to B.D. J.P. and H.C. acknowledge financial support by the Center for Applied Photonics (CAP) at the University of Konstanz, and computer allocations through Grant No. HKN00-10677 from the Jülich Supercomputing Center.

References

1. Zhao H, Yang Y, Janga SC, Kao CC, Zhou Y. Proteins: Struct, Funct Genet. 2014; 82(4):640–647. [PubMed: 24123256]
2. Banerjee A, Santos WL, Verdine GL. Science. 2006; 311:1153–1157. [PubMed: 16497933]
3. Gouge J, Satia K, Guthertz N, Widya M, Thompson AJ, Cousin P, Dergai O, Hernandez N, Vannini A. Cell. 2015; 163:1375–1387. [PubMed: 26638071]
4. Heddi B, Cheong VV, Martadinata H, Phan AT. Proc Natl Acad Sci USA. 2015; 112:9608–9613. [PubMed: 26195789]
5. Buck-Koehntop BA, Stanfield RL, Ekiert DC, Martinez-Yamout MA, Dyson HJ, Wilson IA, Wright PE. Proc Natl Acad Sci USA. 2012; 109:15229–15234. [PubMed: 22949637]
6. Bhattacharyya, SK., Maciejewska, P., Borger, L., Stadler, M., Gulsun, AM., Cicek, HB., Colfen, H. Development of a fast fiber based UV-Vis multiwavelength detector for an ultracentrifuge. In: Wandrey, C., Cölfen, H., editors. Analytical Ultracentrifugation VIII. Vol. 131. Springer; Berlin: 2006. p. 9-22.Progress in Colloid & Polymer Science
7. Pearson JZ, Krause F, Haffke D, Demeler B, Schilling K, Colfen H. Methods Enzymol. 2015; 562:1–26. [PubMed: 26412645]
8. Lamm O. Ark Mat, Astron Fys. 1929; 21B:1–21B. 4.
9. Cao W, Demeler B. Biophys J. 2005; 89(3):1589–602. [PubMed: 15980162]
10. Cao W, Demeler B. Biophys J. 2008; 95(1):54–65. [PubMed: 18390609]
11. Brookes, EH., Boppana, RV., Demeler, B. Computing Large Sparse Multivariate Optimization Problems with an Application in Biophysics. Supercomputing' 06: Proceedings of the 2006 ACM/IEEE Conference on Supercomputing; Tampa, FL. Nov. 11–17, 2006; New York: Association for Computing Machinery (ACM); 2006.
12. Brookes EH, Cao W, Demeler B. Eur Biophys J. 2010; 39:405–414. [PubMed: 19247646]
13. Brookes, E., Demeler, B. Parsimonious Regularization using Genetic Algorithms Applied to the Analysis of Analytical Ultra-centrifugation Experiments. Proceedings of GECCO '07; July 7–11, 2007; London.
14. Brookes, E., Demeler, B. Genetic Algorithm Optimization for obtaining accurate Molecular Weight Distributions from Sedimentation Velocity Experiments. In: Wandrey, C., Cölfen, H., editors. Analytical Ultracentrifugation VIII. Vol. 131. Springer; Berlin: 2006. p. 78-82.Progress in Colloid & Polymer Science
15. Brookes E, Demeler B. Colloid Polym Sci. 2008; 286(2):139–148.
16. Demeler B, Brookes E. Colloid Polym Sci. 2008; 286(2):129–137.
17. Demeler B, Brookes E, Nagel-Steger L. Methods Enzymol. 2009; 454:87–113. [PubMed: 19216924]
18. Gorbet G, Devlin T, Hernandez Uribe B, Demeler AK, Lindsey Z, Ganji S, Breton S, Weise-Cross L, Lafer EM, Brookes EH, Demeler B. Biophys J. 2014; 106(8):1741–1750. [PubMed: 24739173]
19. Demeler B, Nguyen TL, Gorbet GE, Schirf V, Brookes EH, Mulvaney P, El-Ballouli AO, Pan J, Bakr OM, Demeler AK, Hernandez Uribe BI, Bhattarai N, Whetten RL. Anal Chem. 2014; 86(15):7688–7695. [PubMed: 25010012]
20. Kim SJ, Tsukiyama T, Lewis MS, Wu C. Protein Sci. 1994; 3(7):1040–1051. [PubMed: 7920249]
21. Bailey MF, Davidson BE, Minton AP, Sawyer WH, Howlett GJ. J Mol Biol. 1996; 263(5):671–684. [PubMed: 8947567]
22. Laue TM, Senear DF, Eaton S, Ross JB. Biochemistry. 1993; 32(10):2469–2472. [PubMed: 8448106]
23. Demeler, B. Ultrascan—A Comprehensive Data Analysis Software Package for Analytical Ultracentrifugation Experiments. In: Scott, DJ.Harding, SE., Rowe, AJ., editors. Modern

Analytical Ultracentrifugation: Techniques and Methods. Royal Society of Chemistry; London: 2005. p. 210-229.

24. Berke IC, Modis Y. EMBO J. 2012; 31(7):1714–1726. [PubMed: 22314235]
25. Balbo A, Minor KH, Velikovsky CA, Mariuzza RA, Peterson CB, Schuck P. Proc Natl Acad Sci USA. 2005; 102(1):81–86. [PubMed: 15613487]
26. Wong CJ, Launer-Felty K, Cole JL. Methods Enzymol. 2011; 488:59–79. [PubMed: 21195224]
27. Diez AI, Ortiz-Guerrero JM, Ortega A, Elias-Arnanz M, Padmanabhan S, Garcia de la Torre J. Eur Biophys J. 2013; 42(6):463–476. [PubMed: 23512413]
28. Gorbet GE, Pearson JZ, Demeler AK, Colfen H, Demeler B. Methods Enzymol. 2015; 562:27–48. [PubMed: 26412646]
29. Kawakami A, Tian Q, Duan X, Streuli M, Schlossman SF, Anderson P. Proc Natl Acad Sci USA. 1992; 89:8681–8685. [PubMed: 1326761]
30. Wilson R, Ainscough R, Anderson K, Baynes C, Berks M, Bonfield J, Burton J, Connell M, Copsey T, Cooper J, et al. Nature. 1994; 368(6466):32–38. [PubMed: 7906398]
31. Prusiner SB. Annu Rev Microbiol. 1989; 43:345–374. [PubMed: 2572197]
32. Tian Q, Streuli M, Saito H, Schlossman SF, Anderson P. Cell. 1991; 67(3):629–639. [PubMed: 1934064]
33. Le Guiner C, Lejeune F, Galiana D, Kister L, Breathnach R, Stevenin J, Del Gatto-Konczak F. J Biol Chem. 2001; 276(44):40638–40646. [PubMed: 11514562]
34. Kedersha NL, Gupta M, Li W, Miller I, Anderson P. J Cell Biol. 1999; 147(7):1431–1442. [PubMed: 10613902]
35. Kedersha N, Cho MR, Li W, Yacono PW, Chen S, Gilks N, Golan DE, Anderson P. J Cell Biol. 2000; 151(6):1257–1268. [PubMed: 11121440]
36. Emara MM, Liu H, Davis WG, Brinton MA. J Virol. 2008; 82:10657–10670. [PubMed: 18768985]
37. Li W, Li Y, Kedersha N, Anderson P, Emara M, Swiderek KM, Moreno GK, Brinton MN. J Virol. 2002; 76:11989–12000. [PubMed: 12414941]
38. Emara MM, Liu H, Davis WG, Brinton MA. J Virol. 2008; 82:10657–10670. [PubMed: 18768985]
39. Karabudak, E., Colfen, H. The Multiwavelength UV/Vis Detector: New Possibilities with an Added Spectral Dimension. In: Uchiyama, S.Arisaka, F.Stafford, WF., Laue, T., editors. Analytical Ultracentrifugation: Instrumentation, Software, and Applications. Springer; Japan: Tokyo: 2016. p. 63-80.Chapter 5
40. Demeler, B., Gorbet, G., Zollars, D., Dubbs, B. UltraScan-III version 3.3: A comprehensive data analysis software package for analytical ultracentrifugation experiments. 2015. Available via the Internet at: http://www.ultrascan.uthscsa.edu
41. Demeler, B., Gorbet, G. Analytical Ultracentrifugation Data Analysis with UltraScan-III. In: Uchiyama, S.Arisaka, F.Stafford, WF., Laue, T., editors. Analytical Ultracentrifugation: Instrumentation, Software, and Applications. Springer; Japan: Tokyo: 2016. p. 119-143.Chapter 8
42. Cantor CR, Warshaw MM, Shapiro H. Biopolymers. 1970; 9:1059–1077. [PubMed: 5449435]
43. Fasman, GD., editor. Handbook of Biochemistry and Molecular Biology, Vol. 1: Nucleic Acids. 3rd. CRC Press; Cleveland, OH: 1975. p. 589
44. Lawson, CL., Hanson, RJ. Solving Least Squares Problems. Prentice—Hall; Englewood Cliffs, NJ: 1974.
45. Walter J, Sherwood PJ, Lin W, Segets D, Stafford WF, Peukert W. Anal Chem. 2015; 87(6):3396–3403. [PubMed: 25679871]
46. Demeler B. Curr Protoc Protein Sci. 2010:7.13.1–7.13.24. [PubMed: 20814934]

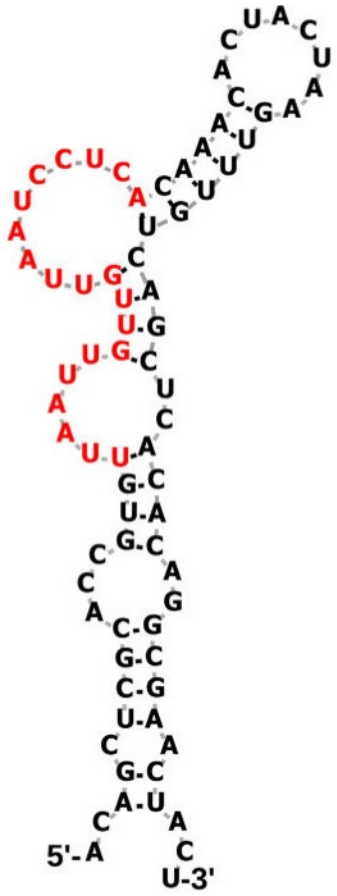

Figure 1.
Predicted secondary structure of the 75 nucleotide WNV-RNA. The sequence of the 20 nucleotide long central loop region of the WNV fragment is marked in red.

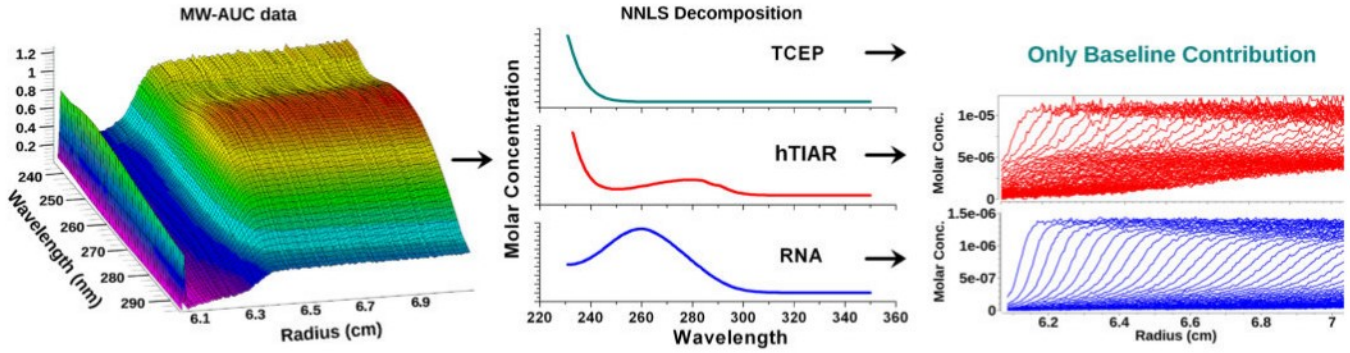

Figure 2.

NNLS decomposition of MWL-AUC data into their spectral constituents. Primary four-dimensional MWL-AUC data (left, only one time point is shown, the meniscus is visible at the left edge of the radial range) are decomposed into their spectral constituents (center), resulting in spectrally separated three-dimensional (3D) datasets (right). Each dataset only reflects the hydrodynamic contributions of one of the constituents, hTIAR and WNV-RNA, which have different chromophores in this case. The TCEP absorbance contribution must be considered in the spectral decomposition; however, since it does not sediment, it only contributes to the baseline, and a hydrodynamic analysis is not necessary.

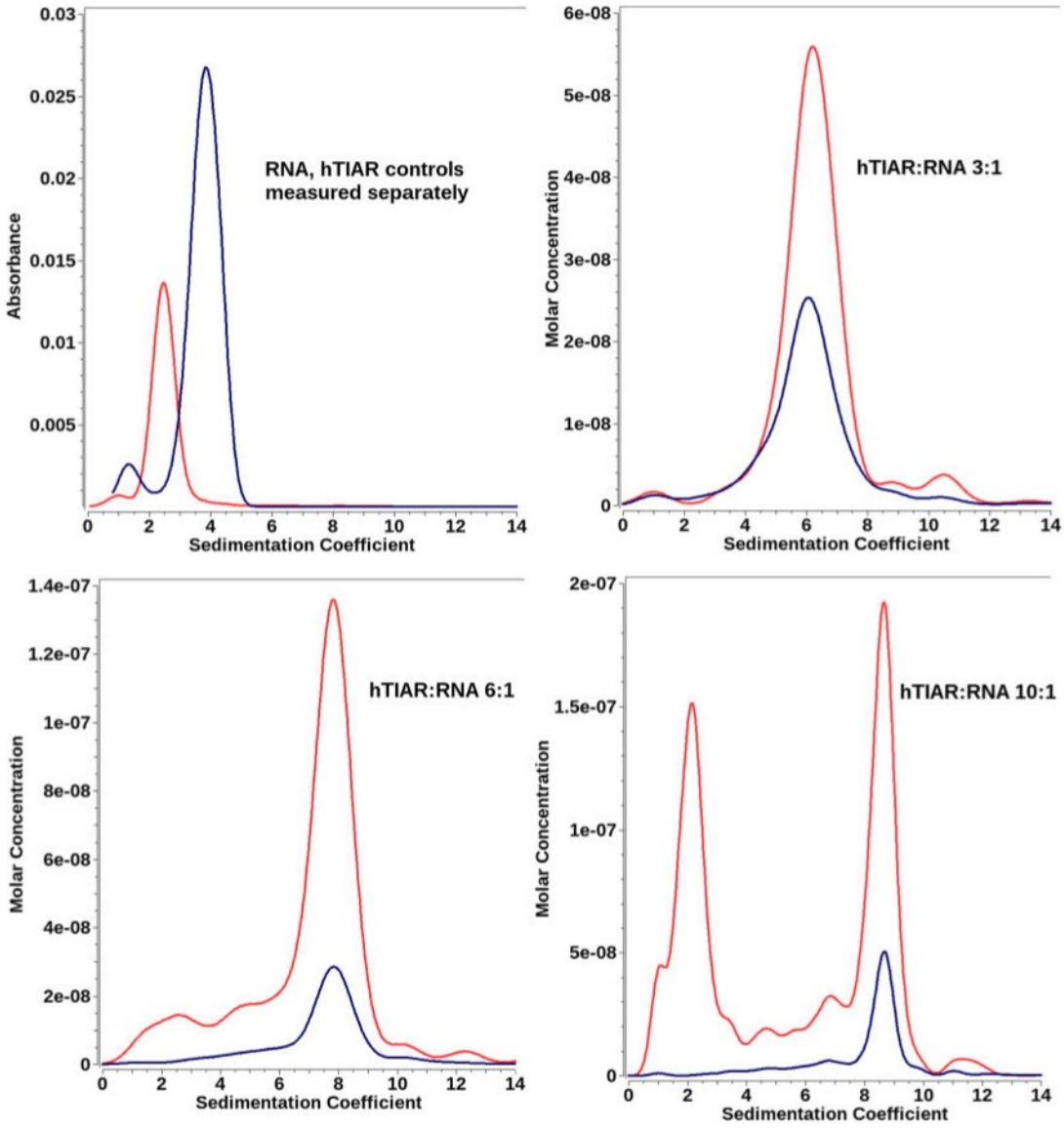

Figure 3.

Global 2DSA-Monte Carlo models obtained from decomposed RNA and hTIAR datasets at different molar mixing ratios. Separate hTIAR and RNA controls (upper left), hTIAR:RNA 3:1 (upper right), hTIAR:RNA 6:1 (lower left), and hTIAR:RNA 10:1 (lower right). All plots show the protein data in red and the RNA data in blue. A clear shift to higher-molecular-weight complex formation is observed as the protein concentration is increased. At the highest ratio (10:1, lower right), the excess unbound protein appears as a peak at the same position as the free hTIAR control (upper left). Broad peaks indicate the presence of a reaction boundary, and absence of a free hTIAR peak, except when added in excess, indicates tight binding between hTIAR and WNV RNA. The control experiments and the 10:1 mixtures were performed at hTIAR and RNA loading concentrations of 11.6 μM and 1.16 μM, respectively. All plots are shown as $g(s)$ distributions with dC/ds plotted on the Y-axis in the indicated units.

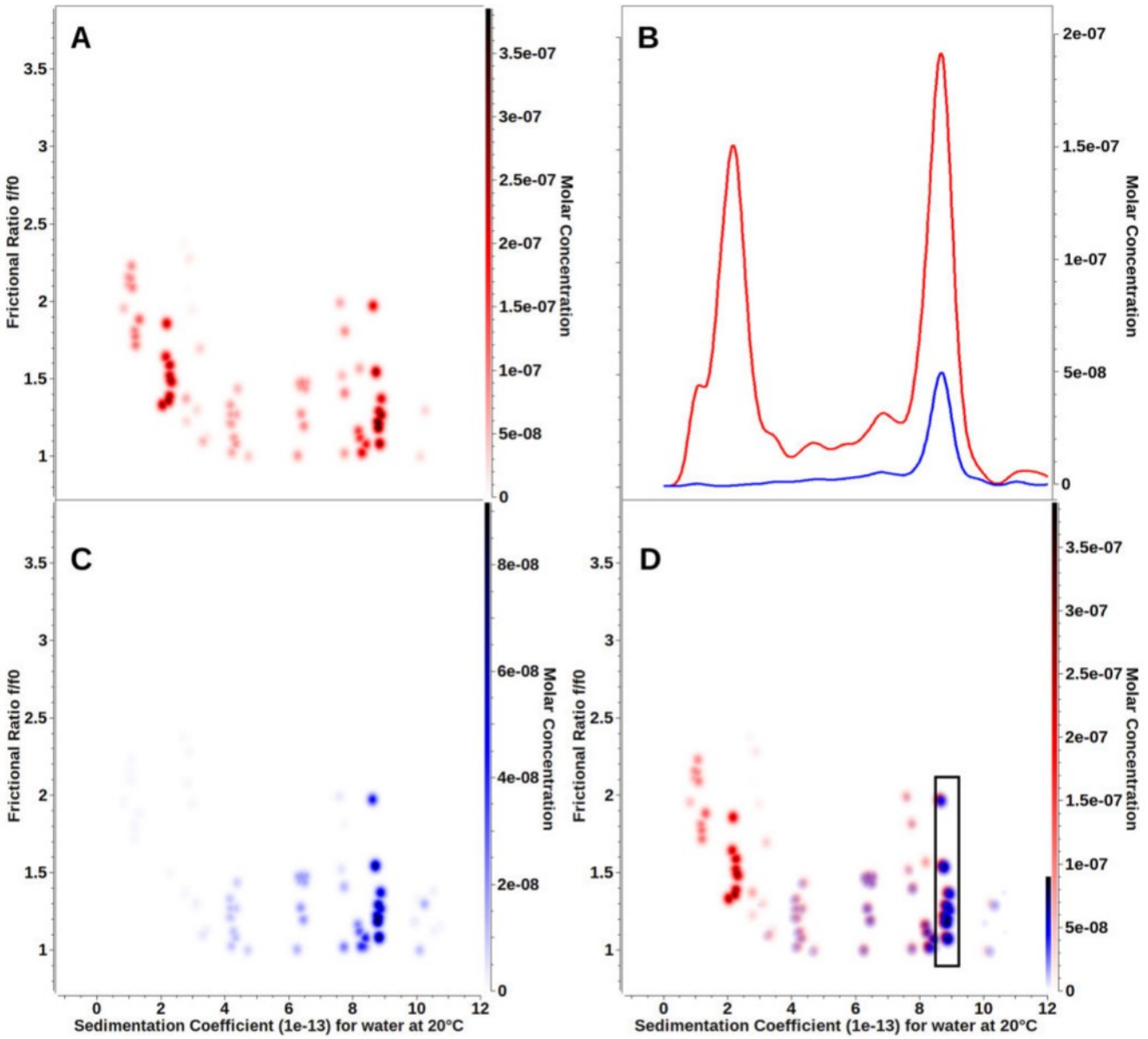

Figure 4.

Global genetic algorithm—Monte Carlo analysis of the 10:1 protein:RNA mixture. This plot shows the distribution of solutes determined in a global genetic algorithm—Monte Carlo analysis, as a function of the sedimentation coefficient and frictional ratio (red = hTIAR, blue = RNA). (A) hTIAR signal alone, (C) RNA signal alone, and (D) hTIAR and RNA models merged. Each dot represents the amplitude of a fitted solute resolved by anisotropy (frictional ratio, f/f_0) and size (sedimentation coefficient, s_{20}, W). Purple solute points represent the complex. Integration limits for the 8.78 S complex are shown in the black box. The confidence limits for the frictional ratio are fairly broad, reflecting limits in radial resolution and limited difiusion signal available at the selected rotor speed, especially for the larger components. The anisotropy for free hTIAR is unreliable, since a partial specific volume consistent with 4:1 hTIAR:RNA was assumed for all species in this analysis.

Intermediate species appear purple and are found at S = 4 and S = 6, but a detailed analysis is unreliable since their partial concentrations are too low. (B) 2DSA-Monte Carlo analysis for comparison, showing hTIAR and RNA signals overlaid.

Table 1

Integration Results from MWL-AUC Global Analysis of Separated hTIAR and RNA Signals[a]

	hTIAR	RNA	hTIAR:RNA		
			3:1	6:1	10:1
sedimentation coefficient ($\times 10^{-13}$ s)	2.45 (2.36, 2.55)	3.87 (3.61, 4.14)	6.43	7.69	8.78[b] (8.64, 8.92)
measured molar ratio[c]	n/a	n/a	1.63	4.25	4.30
predicted part. specific volume[d]	0.728 mL/g	0.550 mL/g	0.672 mL/g	0.701 mL/g	0.701 mL/g
predicted molar mass[e]	31.9 kDa	23.7 kDa	75.7 kDa	159.3 kDa	160.9 kDa
measured molar mas[f] ($\times 10^3$ Dalton)	31.9 kDa (20.5, 43.2)	22.9 kDa (19.8, 25.9)	N/D[g]	N/D[g]	152.7 kDa (66.5, 237.8)

[a] These values were obtained from integration of pseudo-3D plots of the sedimentation/frictional ratio distributions (see Figure 4). The predicted molar mass of a 4:1 complex is 151.3 kDa, in good agreement with the measured value of 152.7 kDa. All measured values represent the arithmetic mean of the Monte Carlo analysis. Values in parentheses are the 95% confidence intervals from the Monte Carlo analysis.

[b] This is the sedimentation coefficient observed in a global genetic algorithm—Monte Carlo fit of both the TIAR and RNA datasets for the species that is identical in both datasets. This species is co-migrating and, therefore, represents the complex.

[c] Concentrations are integrated based on the appearance of any species within the selected regions from the pseudo-3D plots of s vs $f/f0$ (see Figure 4). Since concentrations are already given in molar units, the molar ratios are simply derived from the partial molar concentrations within the regions selected for integration.

[d] Partial specific volume (PSV) values for the complexes are estimated based on the measured molar ratio and the weight fraction of protein and RNA using 0.728 mL/g for TIAR (as calculated by UltraScan from TIAR protein sequence) and an assumed PSV of 0.55 mL/g for RNA (see H. Durchschlag, "Specific volumes of biological macromolecules and some other molecules of biological interest". In *Thermodynamic Data for Biochemistry and Biotechnology*; H.-J. Hinz (Ed.); Springer: Berlin, 1986; pp 45–128).

[e] Masses are predicted based on the observed molar ratios and protein/RNA sequence. The reliability of absolute molar mass transformations of the hydrodynamic data is dependent on the accuracy of the partial specific volume and the precision of the hydrodynamic measurements. Monte Carlo statistics are used to provide estimates of the error of hydrodynamic measurements. The PSV for each species is estimated and can be a considerable source of error; therefore, the molar masses listed here should be considered to be approximate.

[f] The sedimenting species observed for ratios of 3:1 and 6:1 show broad peaks (see Figure 3), indicative of a reaction boundary involving multiple species. The sedimentation and diffusion coefficients corresponding to the peak represent the weight-average sedimentation coefficient and the gradient average diffusion coefficient for all species observed at the highest point of the broad peak.

[g] N/D = not determined.